JGR Atmospheres

RESEARCH ARTICLE
10.1029/2021JD036051

# Four Year Study of the Schumann Resonance Regular Variations Using the Sierra Nevada Station Ground-Based Magnetometers

**J. Rodríguez-Camacho[1], A. Salinas[2], M. C. Carrión[1], J. Portí[1], J. Fornieles-Callejón[2], and S. Toledo-Redondo[3]**

[1]Department of Applied Physics, University of Granada, Granada, Spain, [2]Department of Electromagnetism and Matter Physics, University of Granada, Granada, Spain, [3]Department of Electromagnetism and Electronics, University of Murcia, Murcia, Spain

**Key Points:**

- Long term analysis of the Schumann resonance (SR) records at Sierra Nevada, from March 2013 to February 2017
- The results obtained partially confirm the general aspects of the long-term evolution of the SRs, but new aspects appear
- Recent results on the influence of the El Niño phenomenon and the solar cycle on the SRs are confirmed

**Correspondence to:**
A. Salinas,
asalinas@ugr.es

**Citation:**
Rodríguez-Camacho, J., Salinas, A., Carrión, M. C., Portí, J., Fornieles-Callejón, J., & Toledo-Redondo, S. (2022). Four year study of the Schumann resonance regular variations using the Sierra Nevada station ground-based magnetometers. *Journal of Geophysical Research: Atmospheres*, *127*, e2021JD036051. https://doi.org/10.1029/2021JD036051

Received 17 OCT 2021
Accepted 11 MAR 2022

**Author Contributions:**
**Conceptualization:** J. Rodríguez-Camacho, A. Salinas, M. C. Carrión, J. Portí, S. Toledo-Redondo
**Formal analysis:** J. Rodríguez-Camacho, A. Salinas, M. C. Carrión, J. Portí
**Funding acquisition:** M. C. Carrión, J. Fornieles-Callejón
**Investigation:** J. Rodríguez-Camacho, A. Salinas, M. C. Carrión, J. Portí, J. Fornieles-Callejón, S. Toledo-Redondo
**Methodology:** A. Salinas, J. Portí, J. Fornieles-Callejón, S. Toledo-Redondo
**Project Administration:** M. C. Carrión, J. Fornieles-Callejón
**Software:** J. Rodríguez-Camacho
**Supervision:** J. Portí, J. Fornieles-Callejón



**Abstract** We present a study of the Schumann resonance (SR) regular variations (March 2013–February 2017) using the ground-based magnetometers from the Sierra Nevada station, Spain (37°02′N, 3°19′W). The study is based on the fitting parameters obtained by the Lorentzian fit, calculated for each 10-min interval record, namely, peak amplitudes, peak frequencies, width of the resonances, and the power spectrum integral for the first three SR modes. We consider three time-scales in the study: seasonal, monthly, and daily variations. The processed data collected by the Sierra Nevada station are also made public with this work. The general characteristics of the long-term evolution of the SR are confirmed, but discrepancies appear that require further study comparing recent measurements from different stations. Signatures of the influences of the El Niño phenomenon and the solar cycle to SR have been found.

## 1. Introduction

The Schumann resonances (SRs) are related to the propagation of the electromagnetic (EM) field generated mainly by lightning events in the EM cavity delimited by the lower ionosphere and the Earth's surface. This EM field belongs to the extremely low frequency (ELF) band of the EM spectrum, which goes from a few hertz to around 50 Hz, and its spectrum shows resonances at certain frequencies. This phenomenon is called SRs. In addition to the lightning events produced in thunderstorms, there are some other phenomena that may contribute to the SRs, such as the transient luminous events (TLEs) (Price, 2016).

The SR were theoretically predicted by Schumann (1952) and measured for the first time by Balser and Wagner (1960). A historical review of the SRs and of Schumann can be found in Besser (2007), which shows a review of relevant works about the physical and mathematical concerns of the SRs. A wide review of the theoretical basis and the experimental works aimed at the study of SRs, with an emphasis on the ELF band measurement stations, can be found in Nickolaenko and Hayakawa (2002). More recent works about the SRs are Nickolaenko et al. (2016), Price (2016), and Simões et al. (2012). In Simões et al. (2012), the authors point out as "one of the most challenging issues identifying possible correlations between long term SR variability and climate trends." Also, the books by Nickolaenko and Hayakawa (2014) and Surkov and Hayakawa (2014) make up an extensive bibliographical source about the SRs and the ELF field propagation in the atmosphere. The chapter about the SRs written by Sátori, Mustak, and Williams in Betz et al. (2009) is also of great interest.

The research on the SRs had a resurgence at the end of the twentieth century due to its relation to different climate concerns. In Price (2000), the link between lightning, a primary SRs source, and upper tropospheric water vapor is found. The relation between the average temperature in the tropics and the monthly variations in the SR parameters is shown in Williams (1992). This study was strengthened by Füllekrug and Fraser-Smith (1997), which linked the global lightning activity on a seasonal time scale and the magnetic field variations in the lower ELF range. The SRs are a useful tool to study other climatic phenomena that are influenced by the global thunderstorm activity. In Sátori and Zieger (1999), the variation of the global thunderstorm position southwards in warm El Niño years and northwards in cool La Niña years is observed in the self-consistent behavior of the frequency level and semiannual intensity variations of the first three SR modes. In a latter work, the global lightning activity on the El Niño Southern Oscillation (ENSO) time scale is studied using the SRs together with data from optical transient detector (OTD) and lightning imaging sensor (LIS) satellites in space (Sátori et al., 2009). More recently,

**Validation:** J. Rodríguez-Camacho, A. Salinas, J. Portí, S. Toledo-Redondo
**Visualization:** J. Rodríguez-Camacho, A. Salinas, J. Portí
**Writing – original draft:** A. Salinas
**Writing – review & editing:** J. Rodríguez-Camacho, A. Salinas, J. Portí, S. Toledo-Redondo

Williams et al. (2021) have studied the transition between two Super-Niño periods, occurring in 1997/1998 and in 2015/2016, using data from different stations. The main conclusion is that the variations in the intensity of the SRs may serve as a precursor for these extreme climate events (Williams et al., 2021).

The solar cycle has also an impact on the SRs. In Kulak et al. (2003), it is shown that the first resonant frequency increases when the solar activity increases and that there is a small decrease in the attenuation coefficient of the North-South (NS) component of the horizontal magnetic field measured in the East Carpathian Mountains for 6 years—with some gaps in the recordings. In Sátori et al. (2005), data from three different ELF stations are used to confirm a rise in the frequencies and in the quality factors when the solar activity increases, due to an increase in the X-ray radiation. In addition to the previous results, Ondrášková et al. (2011) uses electric field records to find a reduction of the differences between effective thunderstorm areas during the austral and the boreal summer and thus a prevalence of the semi-annual variations during the years of the deep solar minimum. Toledo-Redondo et al. (2012) showed a possible dependence of the effective reflection height of the Earth-ionosphere cavity and the solar cycle. In Nickolaenko et al. (2015), the 11-year solar cycle is analyzed using data from an ELF station in Antarctica and another ELF station located on the North Pole is added in Koloskov et al. (2020). The experimental observations of these works can be explained by the point source model.

The importance of lightning for climate studies is increasingly recognized (Aich et al., 2018; Williams, 2005). The use of the SRs for inferring the global lightning activity achieved a broad interest, see, for example, Nickolaenko and Rabinowicz (1995) and included bibliography. The relation between the global thunderstorm activity and the diurnal first mode resonant frequency in the vertical electric field component is studied in this work. This connection between the global thunderstorm activity and the SRs also affects the SR amplitudes via annual and semi-annual variations (Nickolaenko et al., 1998, 1999). A similar analysis can be found in Füllekrug and Fraser-Smith (1997), where the profiling of the global thunderstorm activity is made on a seasonal timescale. Another verification of the relation between the SR intensity and the global surface temperature can be found in Sekiguchi et al. (2006), where the annual and semi-annual variations are also studied using principal component analysis (PCA). In Belyaev et al. (1999), the thunderstorms are determined making use of the Poynting vector, obtained with the horizontal components of the magnetic field and the vertical component of the electric field. Some advantages of the use of the Poynting vector are noted in this paper, especially when records from only one station are used. This work finds a night-time peak in African thunderstorm activity.

The thunderstorm activity on the Earth occurs mainly in three regions, located at different longitudes, with a predominance of land areas. These zones are located in Central Africa and Madagascar (African chimney), South and Central America, Caribbean Basin (American chimney), and South-East Asia and Indonesia (Asian chimney), as shown by Christian et al. (2003). These locations have their peak of activity during the local afternoon and they largely modulate the diurnal variations of the SR (e.g., Toledo-Redondo et al., 2010).

First studies of the long-term observations of SR can be found in Sátori (1996) and Sátori and Zieger (1996) with data from the ELF station at the Nagycenk Observatory (47.6°N, 16,7°E), Hungary. These works analyze the SR peak frequencies and amplitudes for the first three modes for 2 years. In Nickolaenko et al. (1998), records for an extra year are added to the previous works and the daily frequency range variations are explored. The seasonal variations of the average daily frequency pattern are also analyzed. A study of the long-term (4 years) diurnal, seasonal and inter-annual variations in the SR parameters can be found in Price and Melnikov (2004). The data are obtained from the ELF station (35.45°E, 30.35°N) near the town of Mitzpe Ramon, in the Negev desert, Israel. The influence of the solar terminator passages on the SR parameters in these records is addressed in Melnikov et al. (2004). In Ondrášková et al. (2007), a summary of more than 4 years of continuous SR monitoring of the vertical electric component at Modra Observatory (48.37°N 17.27°E) in Slovakia is presented. The monthly averaged diurnal variations of the four firsts modes are analyzed. In addition, the diurnal-seasonal variations of the amplitudes, frequencies and quality factors for each year are also studied. The overall pattern of diurnal and seasonal variations in SR frequencies is confirmed from measurements as reported from other observatory sites. Yatsevich et al. (2005) present results from the Lehta station (65°N, 34°E) in Russia from August 1999 to March 2005. In Ouyang et al. (2015) and Zhou et al. (2013), 2 year long records from some low latitude ELF stations in China are examined. The diurnal and seasonal variations in mode amplitudes and frequencies of the first four modes of SR magnetic components are presented.

In this work, the SR regular variations obtained from the ELF station at Sierra Nevada, Spain (Fornieles-Callejón et al., 2015), are analyzed from March 2013 to February 2017. This ELF station records both horizontal magnetic field components, NS and East-West (EW) oriented. The processing of the records is described in Rodríguez-Camacho et al. (2018). With this work, the scientific community is granted access to the processed data from the Sierra Nevada ELF station records. The format of these data is also described in Rodríguez-Camacho et al. (2018). We consider that providing the data is needed to pursue a common goal set by the SR research community and, in general, by the atmospheric electrodynamics research community, which is the creation of a shared database of the different worldwide ELF stations. The 4-year study presented in this paper is intended to carry out an analysis of most the common aspects concerning SR regular variations and comparing these signatures with the results reported by other authors. To the authors knowledge, there is no published study of regular variations of SR corresponding to the years considered in this work. This is especially important for a phenomenon like this, which is extremely difficult to measure and which, in addition, cannot be artificially reproduced in a laboratory. It is also worth noting that the results of the study are also intended to validate the SR measurements that we provide with this work, which is an important point when data are shared with the research community. Finally, it is our opinion that the study presented may help in the use of these data by other authors at the initial stages.

The data used in the analysis presented in this work is the output of the processing scheme applied on the raw data. A brief explanation of this scheme is found in Rodríguez-Camacho et al. (2018). Basically, each file corresponds to the amplitude spectrum of each 10 min interval and the corresponding Lorentzian fitting parameters for each month in the measurement period of the Sierra Nevada ELF station.

This paper is structured as follows: the features and structure of the Sierra Nevada ELF station records are described in Section 2; the diurnal variations of the different SR parameters are studied in Section 3: the seasonal variations are addressed in Section 3.1, and the annual variations extracted from monthly averages are considered in Section 3.2. The time evolution of the SR parameters averaging over a certain number of days, weeks or months is shown in Section 4. Lastly, Section 5 corresponds to the conclusions of this work.

## 2. The Sierra Nevada ELF Station Records

The ELF station is located in the heart of the Sierra Nevada mountains, Granada, Spain, 2,500 m above sea level, in the area surrounding the mountain hut "Refugio del Poqueira" (37°02′N, 3°19′W) (Fornieles-Callejón et al., 2015). The ELF station at Sierra Nevada is equipped with two magnetometers, NS and EW oriented. The signal detected by these magnetometers is amplified, digitized, and registered directly in the time domain. The station is provided with a data acquisition system with a sampling frequency of 256 Hz. The frequency response of the magnetometers ranges from a few tenths of a hertz to 45 Hz. Frequencies from 6 to 25 Hz have been calibrated, thus including the first three SR modes, located around 8, 14, and 21 Hz, which are the target of the Sierra Nevada ELF station. The analog-to-digital converter uses 16 bits to digitize samples in the range $\pm$10 V. The system minimum resolution is therefore $10/215 = 3.052E^{-4}$ V. Saturation limits are fixed at $\pm$9.990 V.

The time domain data are processed using 10-min-long windows. For each window, the average of the amplitude spectra obtained using FFT in 10-s-long intervals is calculated using the Hann window and a 5-s overlap (Welch method). A Lorentzian curve, obtained as a combination of three Lorentzian functions and a straight line, is fitted to the amplitude spectrum between the frequencies 6.35 and 23.75 Hz, named in this paper as the fitting band. It is worth noting that the fitting is applied to the amplitude spectrum as in Price and Melnikov (2004). It is also common the use of the intensity spectrum, instead. This fact must be taken into account when comparing different results, especially with regards to the width of each resonance. For further details of this method, see Rodríguez-Camacho et al. (2018).

As final result of the process, a file containing the following data is generated for each month and sensor, which is generated by Numpy, a Python-based package (http://www.numpy.org):

1. Saturation level (ratio of saturated 10 s long segments for each 10 min interval).
2. Amplitude spectrum for each 10 min interval.
3. Amplitude spectrum of the fitted signal (the fitting curve).
4. Calibrated and fitting frequencies.
5. Fitting parameters.

**Table 1**
*Lowest and Highest Chosen Acceptable Values for the Peak Amplitudes ($P_1$, $P_2$, $P_3$) and the Peak Frequencies ($f_1$, $f_2$, $f_3$) for the Three First Modes and for Each Sensor*

| | $P_1$ (pT/sqrt (Hz)) | | $f_1$ (Hz) | | $P_2$ (pT/sqrt (Hz)) | | $f_2$ (Hz) | | $P_3$ (pT/sqrt (Hz)) | | $f_3$ (Hz) | |
|---|---|---|---|---|---|---|---|---|---|---|---|---|
| | NS | EW | NS | EW | NS | EW | NS | EW | NS | EW | NS | EW |
| Lower limit | 0.13 | 0.10 | 6.80 | 6.70 | 0.10 | 0.08 | 13.18 | 12.82 | 0.08 | 0.08 | 19.15 | 18.40 |
| Upper limit | 0.80 | 0.80 | 8.35 | 8.22 | 0.80 | 0.80 | 15.19 | 14.98 | 0.80 | 0.80 | 21.98 | 22.60 |

6. UTC hour for the beginning of each 10 min interval.

The format is that generated by Numpy, a Python-based package (http://www.numpy.org).

Concerning the Lorentzian fitting function, as explained in Rodríguez-Camacho et al. (2018), there are 11 fitting parameters: three individual mode amplitudes, three resonant frequencies, three Full Widths at Half Maximum (FWHMs), and two parameters corresponding to a linear correcting part (the slope and the intercept). Once this fitting curve has been obtained, we get the maximum amplitudes, $P_i$, and the frequencies at which these maximum values appear, $f_i$, for the $i$th mode ($i$ = 1,2,3). These quantities will be referred to as peak amplitudes and peak frequencies, respectively, and will be used for the long-term analysis as they best describe the global behavior of the SRs. The power spectrum integral (PSI), over the fitting bandwidth (6.35–23.75 Hz), of the magnetic field recorded in each sensor has also been included as a parameter for the study.

As commented above, the study of the regular variations of the SRs is based on the fitting parameters obtained by the Lorentzian fit, calculated for each 10-min interval records. For some intervals, the parameter values are unacceptable. This can be due to different reasons (strong lightning activity near the station, bad performance of the Lorentzian fitting algorithm, etc.). For this reason, a mask is used to discard the 10-min intervals for which the values of the peak amplitudes or the peak frequencies are unacceptable. The chosen acceptable values for the peak amplitudes and for the peak frequencies are shown in Table 1.

In order to have a global picture of the data recorded by the Sierra Nevada ELF station, the PSI is shown in Figure 1 for both sensors. The days are represented in the horizontal axis and the 10 min intervals of the day are represented in the vertical axis. The PSI values are shown using the colormap on the right side of the chart. The dashed white line indicates the dusk and dawn times. Vertical white lines correspond to missing data.

## 3. Diurnal Variations

### 3.1. Diurnal Variations for Seasonal Periods

The peak amplitudes of each horizontal magnetic field component are shown in Figure 2 for each mode through a day (diurnal variations), averaged within each one of the four astronomical seasons for the period of four years (from March 2013 to February 2017). A comparison of the amplitude of each magnetic field component in Figure 2 with those presented in Zhou et al. (2013) from ELF stations located in China shows that latter amplitudes are higher due the proximity of the Maritime Continent (MC) thunderstorms to the Chinese stations. The amplitudes obtained in Sierra Nevada station oscillate between 0.20 and 0.45 pT/sqrt (Hz) whereas in Zhou et al. (2013), they oscillate between 0.4 and 1.2 pT/sqrt (Hz). The different thunderstorm chimneys and their impact on each component of the horizontal magnetic field can be clearly noted. It can be seen that the African thunderstorms are dominant about 1500 UT in the EW component, whereas the thunderstorms in the MC and America are detected in the NS magnetometer with intensity peaks at 1030 and 2000 UT, respectively, although the exact maximum time varies with the season. This general form of the amplitudes for the first mode can be justified by the two-source model that considers a localized storm center which moves following a circle near or defined by the equator and surrounding the entire Earth during the day and another permanent center distributed throughout the line described by the first source. The moving source defines the maximum and minimum hours in the amplitudes while the second source provides an average amplitude level that brings the signal generated by the first source closer to that experimentally observed (Yatsevich et al., 2005, 2008).

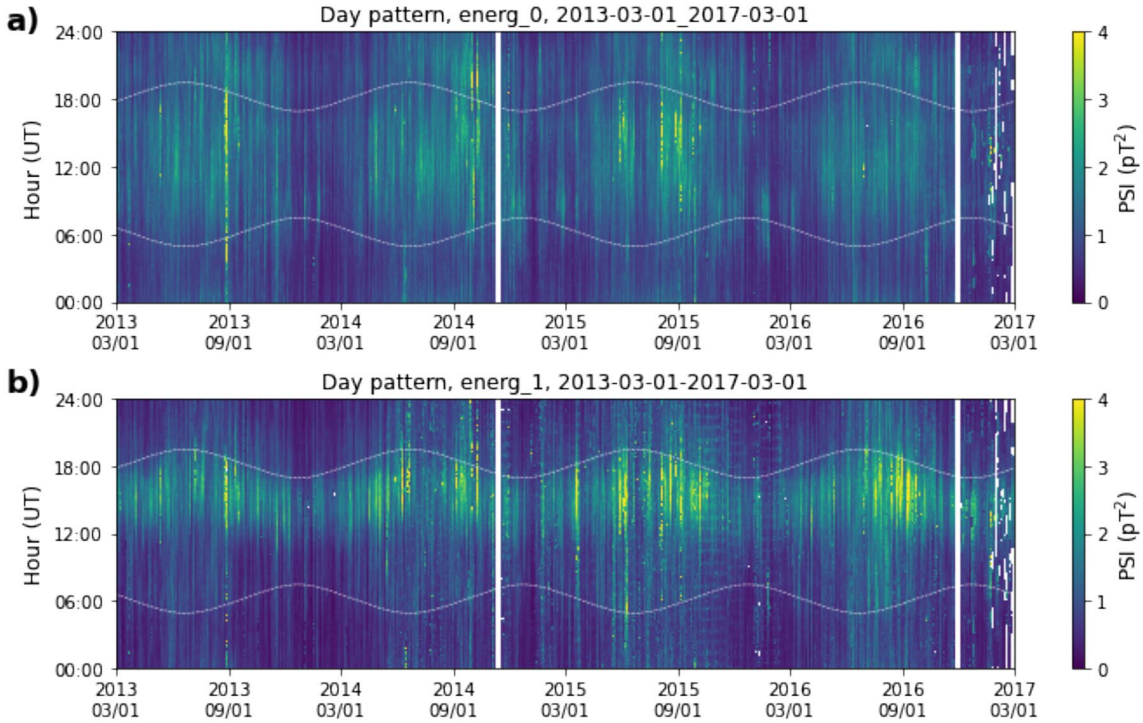


**Figure 1.** Power spectrum integral (PSI) for the recordings at Sierra Nevada extremely low frequency station, from March 2013 to February 2017. The upper chart corresponds to the North-South magnetometer and the lower one to the East-West magnetometer.

In the NS component the MC activity starts rising at 0400 UT and hits a maximum about 1030 UT for the first mode. This maximum amplitude recorded at Sierra Nevada in this sensor may be due to the superposition of the MC thunderstorms and other thunderstorms that would be located at an intermediate distance, like India. In Yatsevich et al. (2008), the peak amplitude for this storm center is between 0800 UT and 1000 UT. Other authors, like Price and Melnikov (2004) and Zhou et al. (2013), report that the maximum amplitude for the first mode about 0800 UT corresponds to the MC thunderstorms but this peak does not appear in the Sierra Nevada data. The reason for this may be due to the effect of the proximity of the Australian and the MC to the antipode point relative to the Sierra Nevada ELF station location or a shift in storm activity to regions closer to the Sierra Nevada station, such as India. For this chimney, the amplitude is dominant in summer, followed by spring, autumn and far below during winter. This situation also occurs for the American thunderstorms, but this chimney shows more activity in autumn than in spring. The time at which this American peak happens has a strong seasonal dependence. The smallest intensity for this chimney is observed in winter, though it is the most active thunderstorm center in winter and for the first mode during the whole day. In addition, throughout the day, a drop in the amplitude of the second and third modes is observed with regard to the first mode, and the second and third modes are very sensitive to the African thunderstorms (between 1500 and 1600 UT). The complicated patterns observed in SR2 (NS) and SR3 (NS) could be explained by the random variation between the source-observer distance (SOD).

For the EW component, which is more sensitive to the African thunderstorms, the amplitude and shape are similar in the three modes. An amplitude peak is observed in the three modes about 1500 UT and it has a stronger activity in summer for the first and the third modes, whereas the second mode is higher in spring. A change in the time of this maximum is observed when the seasons change. It goes from 1600 to 1500 UT from summer, spring, autumn, and winter, and its amplitude also decreases in this order (except in the second mode, for which summer and spring exchange maximum amplitudes as previously noted). This peak in summer, due to the African thunderstorms, cannot be justified by the lightning observations in Blakeslee et al. (2014), where the African thunderstorms have a minimum activity in summer. This discrepancy could be due to the different years used for observation in both studies or also considering the storms of Europe and West Asia (Yatsevich et al., 2008). The EW magnetometer also collects a minor peak about 0600 UT, observed mainly in summer and spring, which

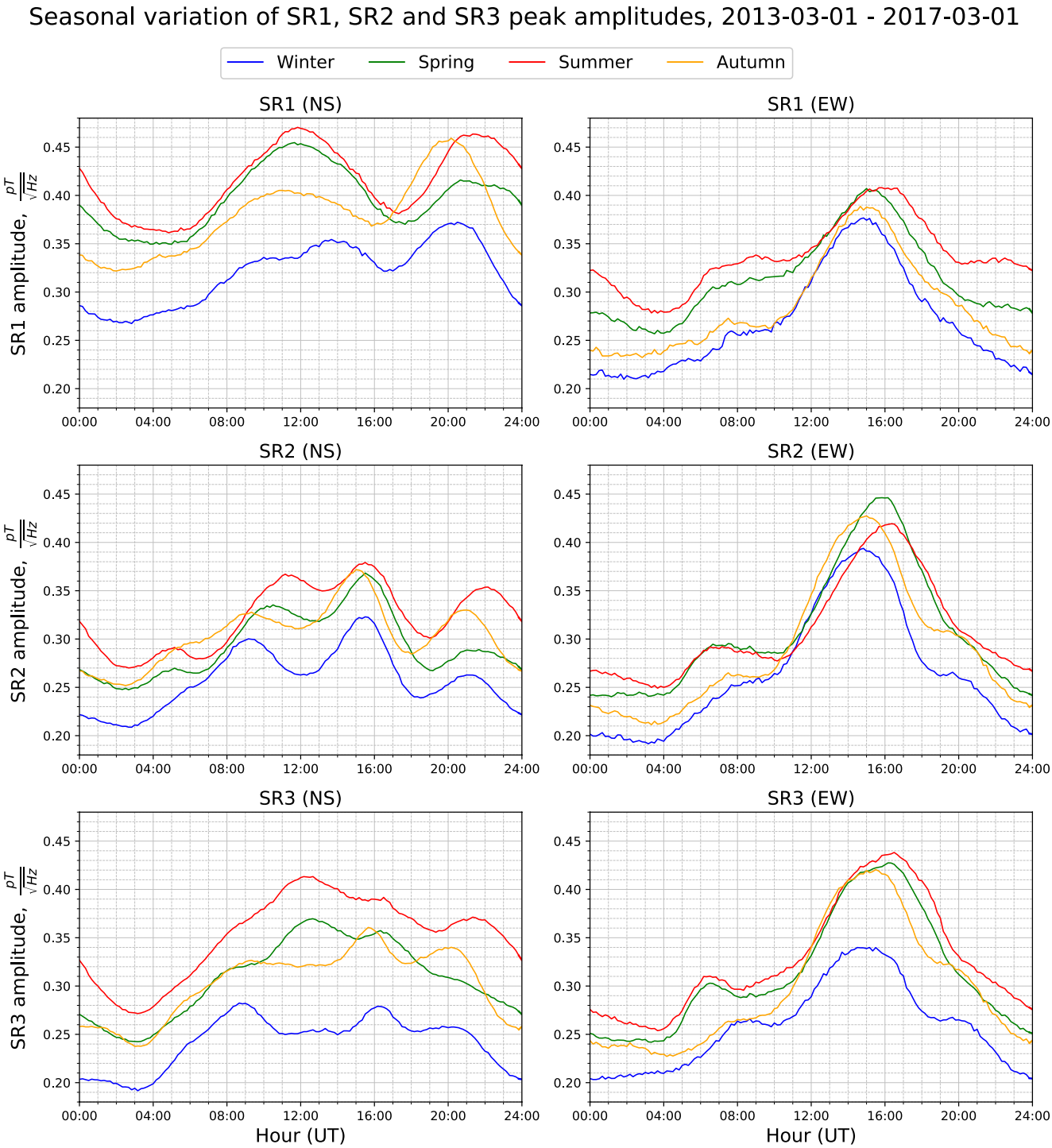


**Figure 2.** Diurnal variations of the peak amplitudes for the three first modes (SR1, SR2, and SR3), in the different seasons over the recording period (2013–2017). The left column corresponds to the North-South magnetometer and the right one to the East-West (EW) magnetometer. Each row corresponds to a different mode (SR1, SR2, and SR3).

could be connected to the nighttime thunderstorms in Africa (Belyaev et al., 1999). This nighttime peak is also present in Price and Melnikov (2004) and Yatsevich et al. (2008).

The diurnal variations of the peak frequencies (the local maximum frequencies) for the first three modes, seasonally averaged, are shown in Figure 3. These variations of the peak frequencies are linked to the source-observer

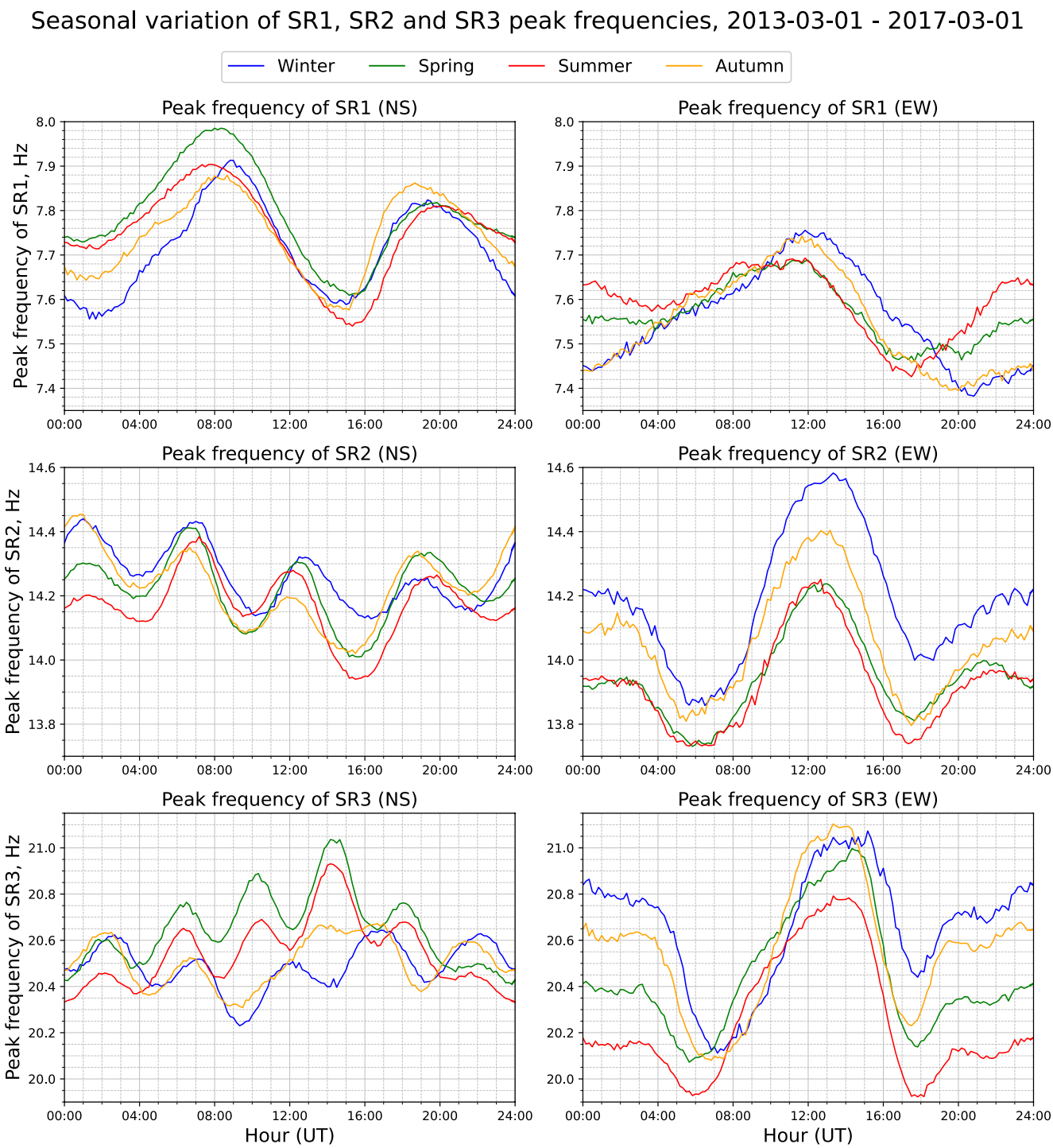


**Figure 3.** Diurnal variations of the peak frequencies for the three first modes, in the different seasons over the recording period (2013–2017). The left column corresponds to the North-South magnetometer and the right one to the East-West magnetometer. Each row corresponds to a different mode (SR1, SR2, and SR3).

geometry (e.g., Nickolaenko & Hayakawa, 2002; or Toledo-Redondo et al., 2010, 2016). Considering a "Hot Spot" or localized source model, described in Nickolaenko and Hayakawa (2014), the peak frequency of the magnetic field for the first mode should have a minimum when the source is closest to the observer and a maximum when the source is farthest from the observer. However, as we will see below, this is only roughly observed for the NS sensor. For both sensors, the minimum and maximum frequencies observed greatly depend on the

mode, the hour of the day and the temporal definitions of the seasons themselves, as it will be shown below. In the Sierra Nevada records, unlike in other ELF stations (Price & Melnikov, 2004; Zhou et al., 2013), there is not a strong seasonal dependence of the diurnal frequency variation. A transition from "winter-type" to "summer-type" diurnal frequency variation is not observed. As noted in Price and Melnikov (2004) and in Yatsevich et al. (2008) an attempt to explain these frequency variations should be done in the future using a theoretical model for a better agreement between the model and the experiment.

The analysis of the peak frequency diurnal variations shows a different behavior for the NS and EW components. For the NS component, the number of maxima and minima observed increases by two for each mode, starting from two maxima and two minima for the first mode. The first mode frequency is highest about 0800 UT and 2000 UT, and lowest about 0300 UT and 1500–1600 UT. This location of maximum and minimum corresponds approximately to that expected according to the SOD with the sources located in Asia and America and it is similar to the one detected by the Letha station presented in Yatsevich et al. (2008). These maxima and minima are also observed in the second mode at the same times, together with two more maxima about 0100 UT and 1200 UT and two more minima about 1000 UT and 2300 UT. In the second mode, more evident distinctions appear among the different seasons, but the general pattern is still conserved. However, for the third mode, there is a clear distinction between the spring-summer seasons and the autumn-winter seasons. It is remarkable that the third mode frequency is highest about 1400 UT in spring-summer while it shows a relative minimum in winter at the same hour. This increase in the number of maxima and minima is also observed in Price and Melnikov (2004).

For the EW component the diurnal peak frequency variation for the three modes reflects a rather similar pattern, with a remarkable maximum value. The highest frequency appears at 1200 UT, 1300 UT, and 1400 UT, respectively, for each mode in all seasons. Also, a relative maximum is seen around 0000 UT that, for the first mode, is highest in summer and it is smaller, in a decreasing order, in spring, autumn and winter. For the second and third modes, the order is reversed. Minimum frequencies appear about 0600–0700 UT and 1800 UT for the second and the third modes, while for the first mode there is a clear minimum that occurs about 1700 UT in spring-summer and about 2000 and 2100 UT in autumn and winter, respectively. For this sensor, a minimum should be obtained when storms in Africa are most active. However, we can see that this peak is displaced and also this displacement increases with the autumn and winter seasons.

Regarding the widths of the resonances, they show a more fluctuating behavior than the other parameters. In Figure 4, it can be observed that these fluctuations do not depend much on the season and they are similar for both the NS and EW components. The widths are higher for the EW sensor than for the NS sensor for all the modes. It is lowest in the second mode. For the third mode, during winter, several peaks are observed in the width for the EW sensor: it shows values around or higher than 7 Hz, whereas it shows values between 3 and 3.5 Hz in the other seasons.

An analysis of the PSI is shown in Figure 5 for the different seasons. This parameter is sensitive (in a nonlinear way) to the contributions of the three modes, thus it can be a good indicator to be compared to the direct lightning observations from satellites, like that presented in Blakeslee et al. (2014). As in previous results, we can observe in sensor NS the activation of the thunderstorms in North America in the summer and autumn and in South America in winter around 2100 UT; with respect to the Asian thunderstorms (mainly observed in the NS sensor), they are maximum in summer and spring, and we can also see the activation of Australian thunderstorms in winter around 0800 UT. There are, though, some differences between the observations via satellite and those obtained from the SRs: the peak detected in the EW sensor around 0500 UT in the summer and spring (which possibly comes from African thunderstorms, as it has been commented previously) does not appear in Blakeslee et al. (2014); in the EW sensor, the African thunderstorms cause a maximum around 1600 UT in the (boreal) summer, whereas in Blakeslee et al. (2014), they show a minimum activity in the (boreal) summer. Figure 5 is similar to Figure 6a and 6b of Price and Melnikov (2004). The latter represents the sum of the amplitudes of each of the first three modes and presents diurnal variations with averages for each year.

The concept of EM seasons was introduced by Sátori (2003) and Sátori et al. (2003) and a definition based on SR measurements and a numerical model is made in Nickolaenko et al. (2015). The summer is set to last from June to September, the winter is set to last from February until March, and the rest of months belong to the spring or to the autumn. The diurnal variations seasonally averaged, taking into account the setting of the seasons made by Nickolaenko et al. (2015), are shown in Figure 6 for the PSI parameter. It is interesting to compare the diurnal

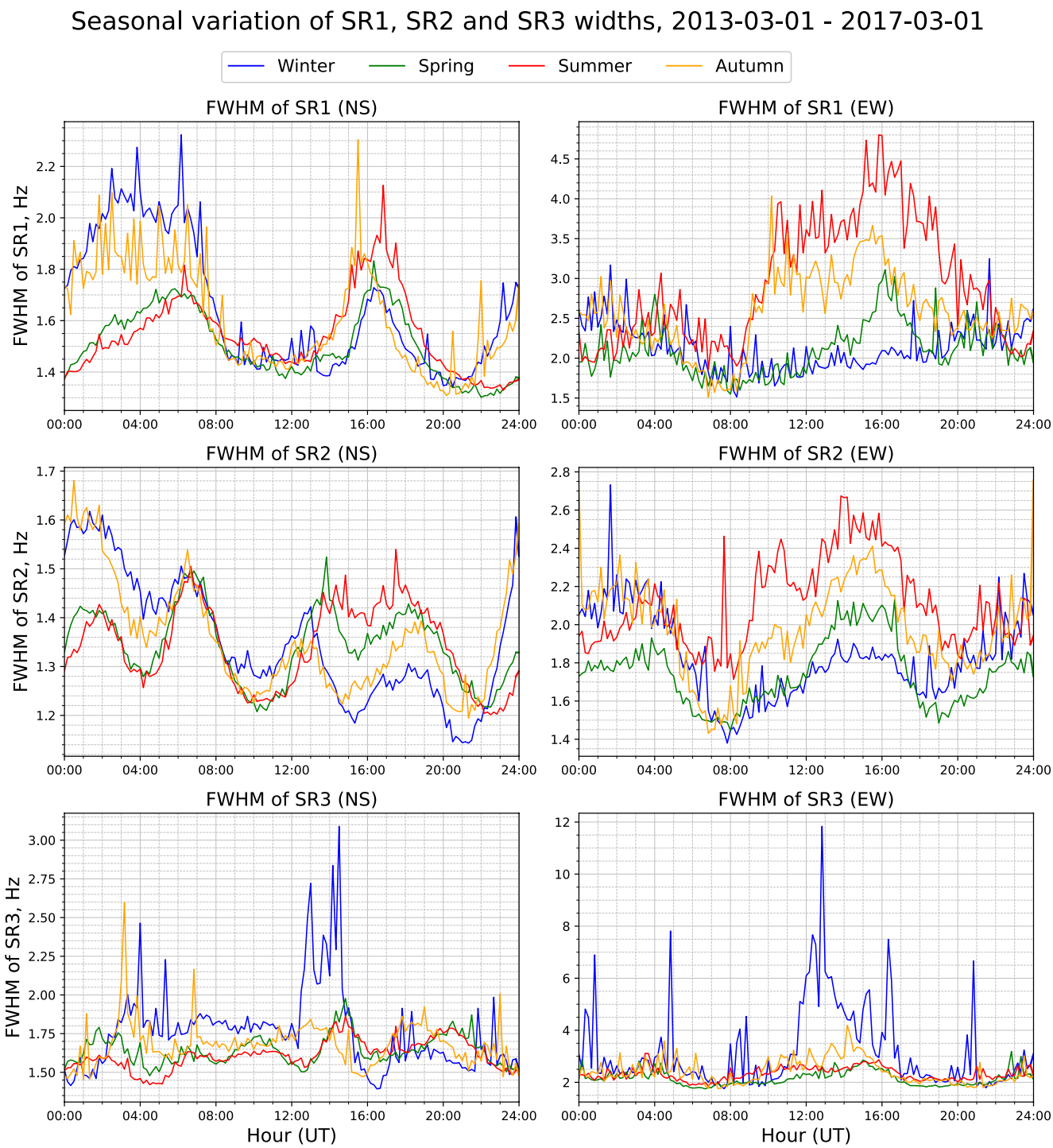


**Figure 4.** Diurnal variations of the Full Widths at Half Maximum of the resonances for the three first modes, in the different seasons over the recording period (2013–2017). The left column corresponds to the NS magnetometer and the right one to the East-West magnetometer. Each row corresponds to a different mode (SR1, SR2, and SR3).

variations of the different parameters for both sets of seasons, the astronomical seasons in Figure 5 to the electromagnetic seasons in Figure 6. It can be noted that the seasonally averaged diurnal variations are in phase for the different seasons, that is, the maxima and minima appear at the same UT hour for all seasons. A clear difference between EM summer and the other EM seasons is also clearly shown.

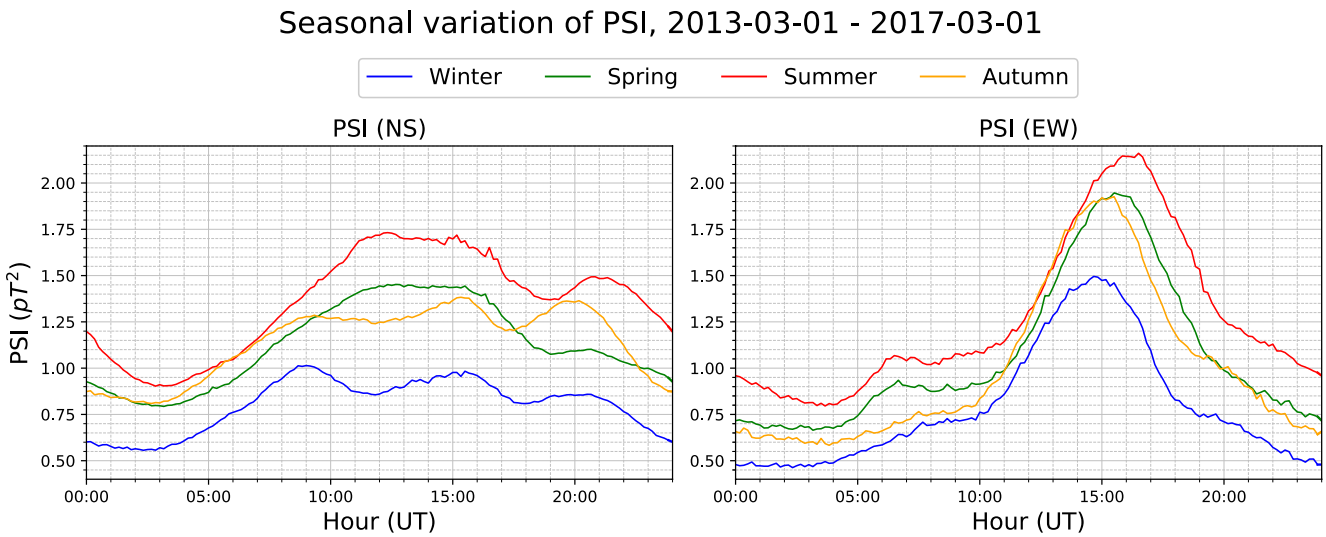


**Figure 5.** Diurnal variations of the power spectrum integral for the different seasons over the recording period (2013–2017), in the frequency range 6.35–23.75 Hz. The left chart corresponds to the North-South magnetometer and the right one to the East-West magnetometer.

### 3.2. Annual Diurnal Variations

Another interesting indicator is the study of the diurnal variations of a parameter for a specific month for different years. The diurnal variations for the months of September, December, and February are shown in Figure 7 over several years for which the recordings at the Sierra Nevada station are available. The parameter plotted is the first mode peak amplitude for each one of the horizontal components. This figure is similar to (c)–(e) in Figure 3 in Williams et al. (2021). More precisely, Figure 7 is similar to the plot of the data from the Eskdalemuir station, located in a similar latitude to the Sierra Nevada station, with the only difference that the amplitude in the EW component was slightly higher in February 2016, than in 2014. These results confirm the conclusions on an intensification of the SRs during the transition months that precede the super El Niño episode that happened at the end of 2015 and the beginning of 2016. We can note an intensification of the, SRs in September 2014, with a maximum intensification from December 2014 to February 2015. We can also confirm a decrease in the thunderstorm activity in the declining phase of the phenomenon in February 2016, though in Sierra Nevada this decrease is lower in the EW sensor than that observed in the Eskadalemuir station (Williams et al., 2021).

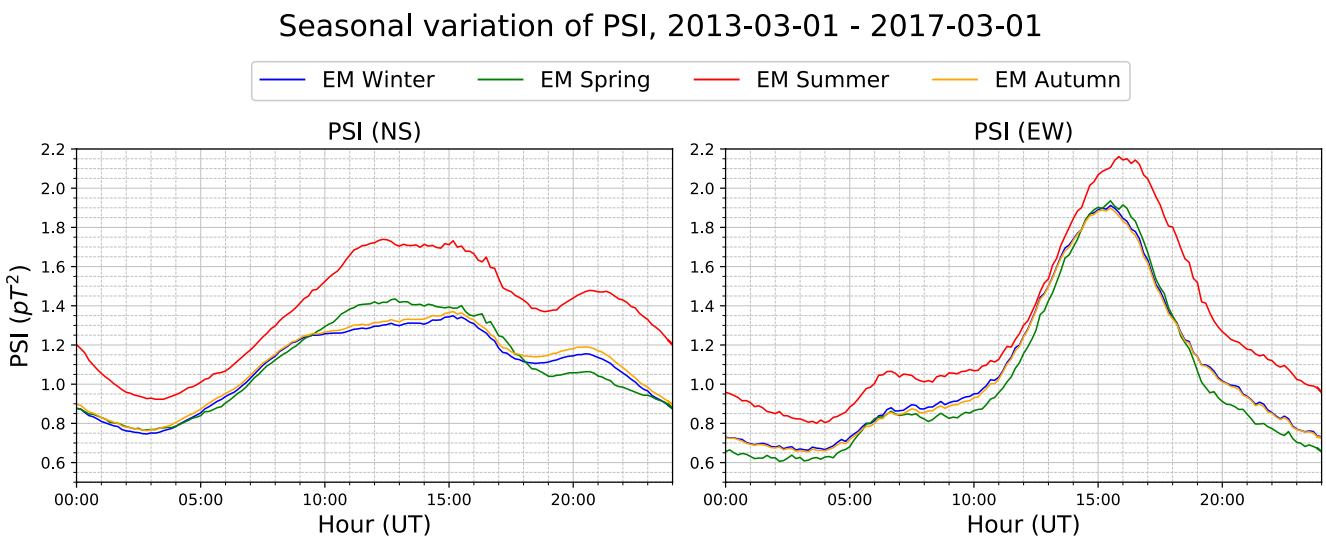


**Figure 6.** Diurnal variations of the power spectrum integral for the different electromagnetic seasons over the recording period (2013–2017). The left chart corresponds to the North-South magnetometer and the right one to the East-West magnetometer.

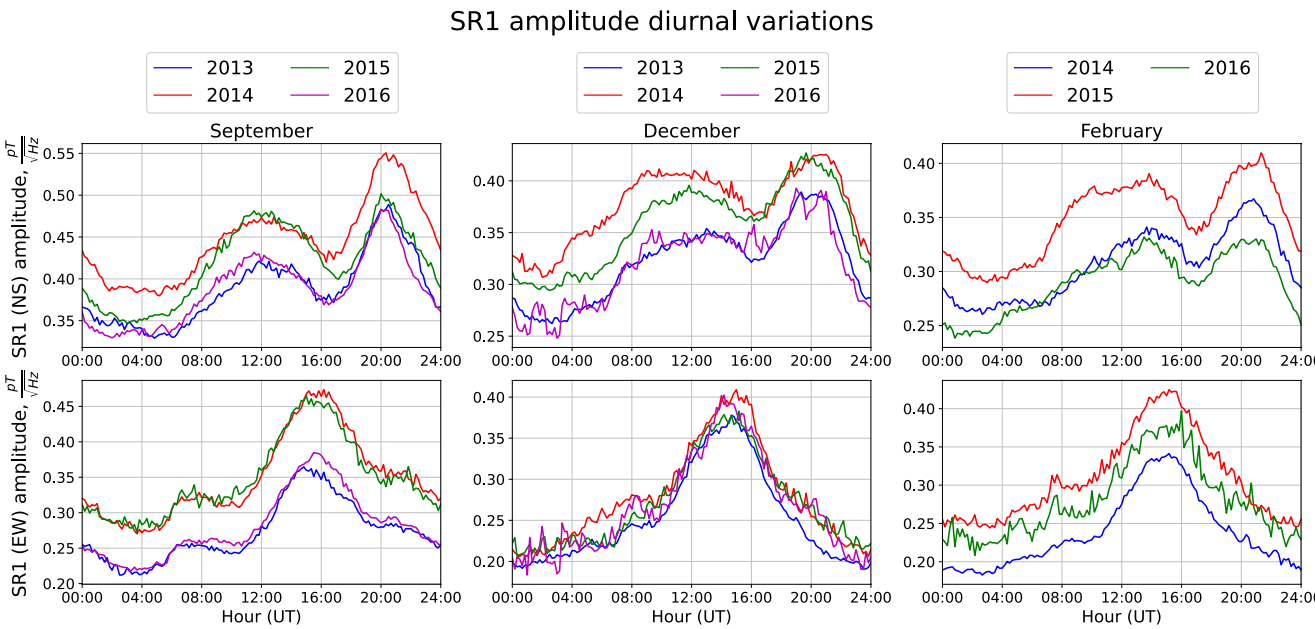


**Figure 7.** First mode peak amplitude annual diurnal variations for each one of the horizontal components for the months of September, December, and February, for several years.

Another interesting result is related to the PSI. The NS component is shown in Figure 8, where two different patterns can be noted. One of them corresponds to autumn-winter, where the three main thunderstorm centers are observed, with a predominance of the MC center in winter and American center in autumn. The other pattern corresponds to the summer behavior, where the African thunderstorms are dominant. However, in Figure 9 showing the PSI for the EW component—the most sensitive to Africa—and over the different years of recording, the pattern repeats for all the months with only a slight reduction in the maximum during winter months, especially in December and January.

It can be noted in Figures 8 and 9 that the differences among the years persist throughout the whole day, that is, when a parameter is higher than usual for a certain year, it is higher for every time of the day. This feature is observed in all the parameters analyzed, even those not shown in these figures. This could indicate that there is some mechanism that affects SR on a global scale.

## 4. Daily Variations

After studying the diurnal variations, the daily evolution of the parameters over time will be addressed. In contrast to the diurnal variations, which provide average information on specific moment of the day, as regards the daily variations, we obtain a unique average value for each day and this value is again averaged over a larger time span, which will range from 1 to 6 months in our study. In practice, it is a mean value for the quantity during this larger period, disregarding hourly details. In all the cases presented below, the daily variation of this average is shown for the 4 years for which the records are available.

The PSI for both NS and EW sensors, averaged every 30 days, is shown in Figure 10. Three clear periods can be observed. The first one goes from 2013 to the beginning of 2015, where the NS component amplitude exceeds the EW one. The second period extends over almost the whole 2015, where both components have the same amplitude. The third period begins in 2016 for which the EW amplitude exceeds the NS one. It is difficult to determine which thunderstorms centers are most active from the PSI observations, since the contribution of the different modes varies with each center due to the source-observer distance. But it is clear that from the end of 2014 to the beginning of 2016 there was a transition period in which the source of the SRs changed. This change may be related to a transition year from the Niña period to the Super El Niño phenomenon of 2015/2016 reported in Williams et al. (2021).

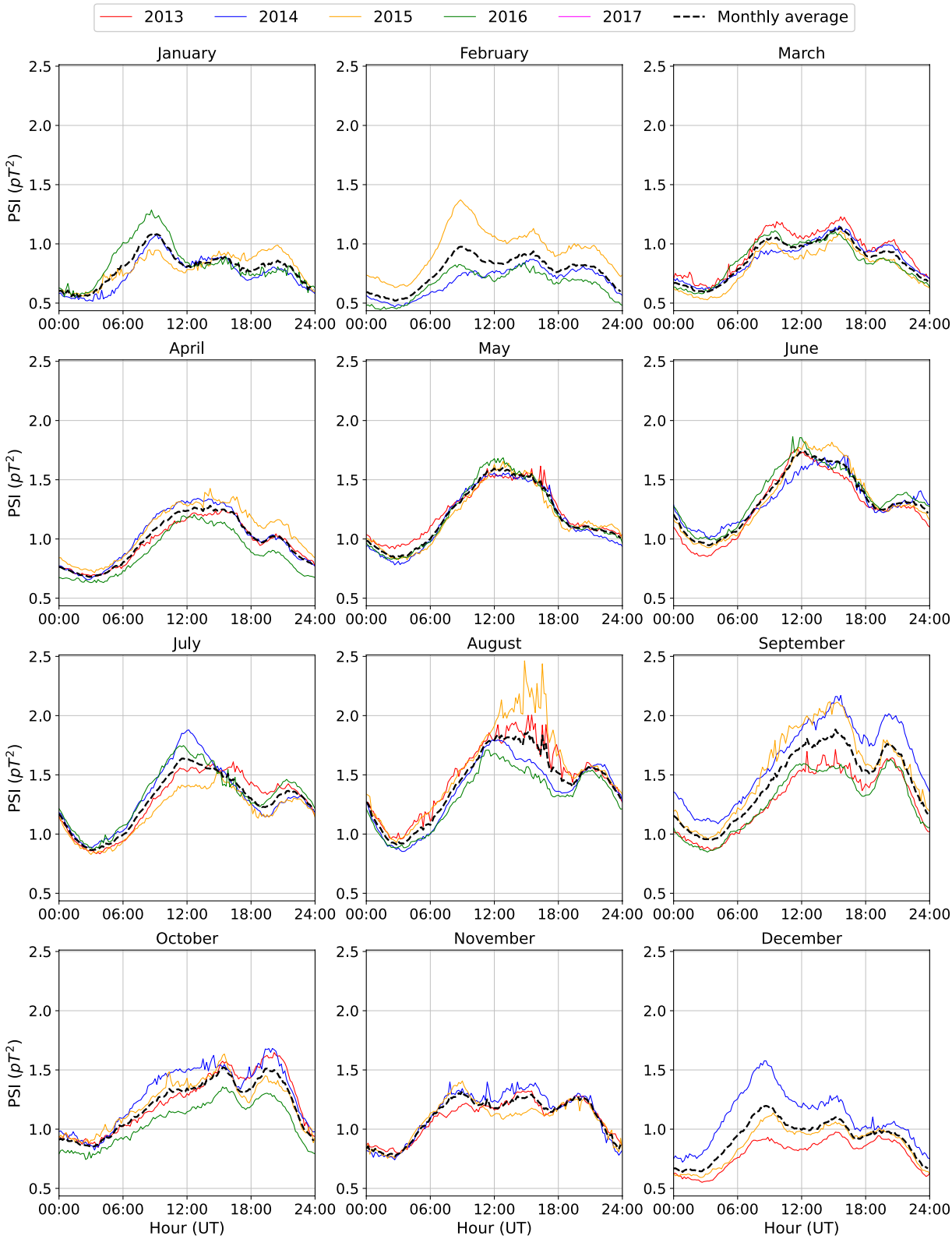


**Figure 8.** Monthly averaged diurnal variations of the power spectrum integral during the whole recording period of the station for the North-South sensors.

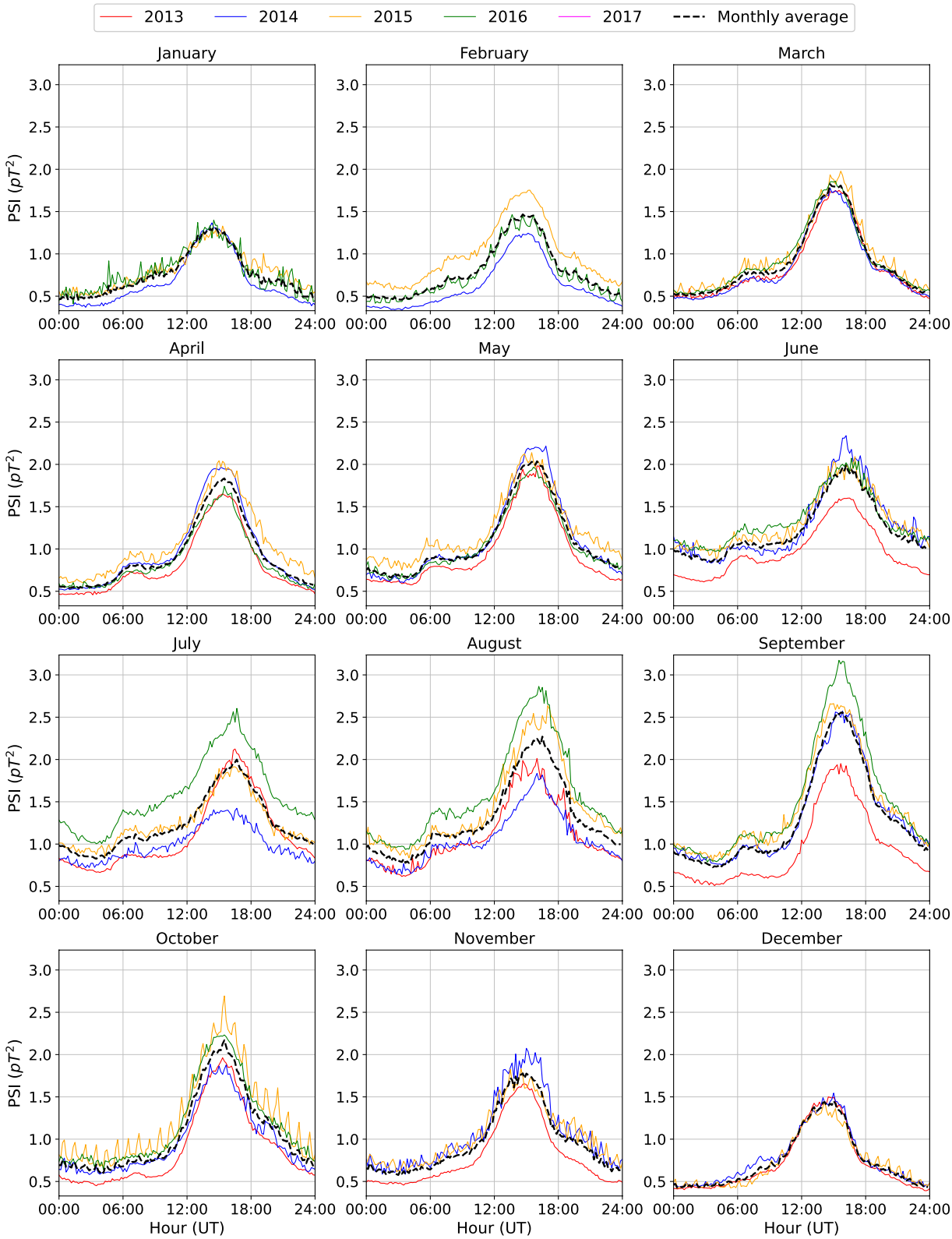


**Figure 9.** Monthly averaged diurnal variations of the power spectrum integral during the whole recording period of the station for the East-West sensors.

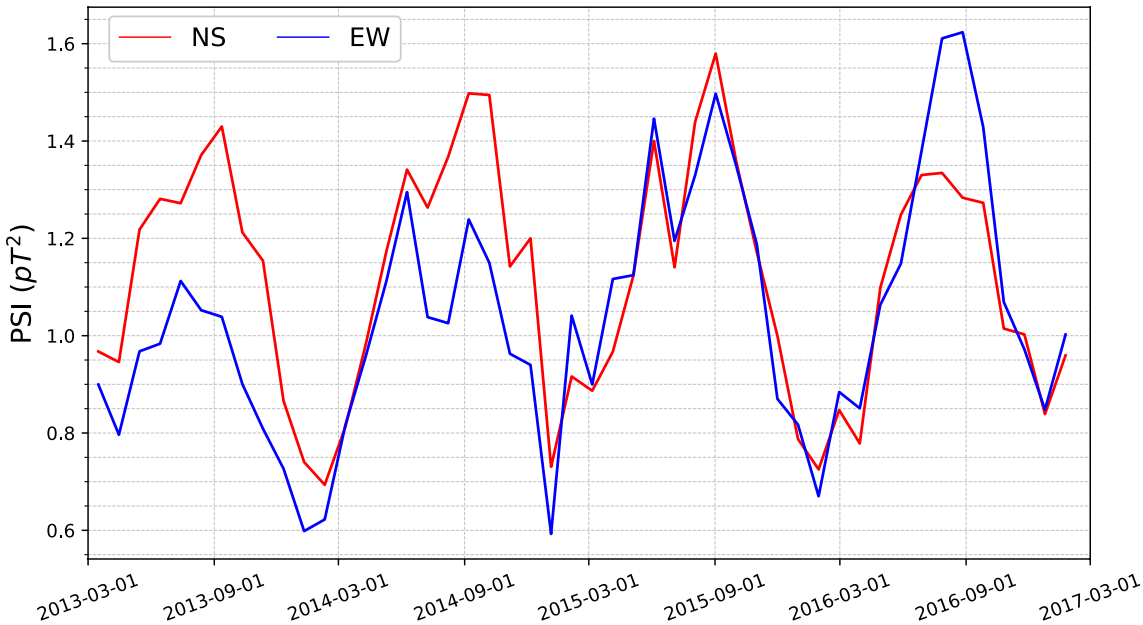


**Figure 10.** Power spectrum integral averaged every 30 days, for both North-South (red) and East-West (blue) components.

Another aspect to point out in Figure 10 is the increase in the maximum and minimum values of the PSI in both sensors that occurs during the 4 years of measurements. This fact could be related to global warming (Williams et al., 2019). However, as a preliminary step to this study, it would be necessary to confirm the trend of the PSI measured at Sierra Nevada with data from other stations. It is a pending work for the future, once a joint database of different ELF stations is available.

In Koloskov et al. (2020) the inter annual variations of the first mode resonant frequency is correlated to the 11-year cycle solar activity, during a period of large solar activity (2011–2017), which had a rise in 2014. The mode peak frequency variations are shown in Figure 11 for the three modes, semi-annually averaged. It can be seen that the variations and the evolution for the first mode, upper row of Figure 11, is very similar to that in Figure 1c in Koloskov et al. (2020).

Regarding the peak frequencies for the second and third modes it can be noted, in the semi-annually averaged data, that the frequencies also tend to decrease during the years except for the sensor EW in the third mode, when a notable rise occurs in 2016, but it is soon followed by a new decreasing trend. In these modes, in particular for the EW sensor, a steady semi-annual periodicity is observed in the maxima and the minima of the peak frequency.

Another relevant concern about the time evolution of the different parameters is the diurnal variation of the minimum to maximum range of peak amplitudes and peak frequencies, Figures 12 and 13, respectively. We can see that, for a 30 days average, the variations that show all the parameters in all the modes are higher for the EW sensor than for the NS sensor. In the EW sensor, we can clearly see an increase in the variations of the peak frequency of the second mode in the year 2015. It can also be noted that no annual variations are observed in any parameter.

## 5. Conclusions

In this work, we present a detailed analysis of the regular variations of the SRs during the period March 2013–February 2017, using the Sierra Nevada station (37°02′N, 3°19′W) ground-based magnetometers. Each component of the magnetic field measured has been processed by fitting Lorentzian functions to the amplitude spectrum, in a bandwidth of (6.35–23.75) Hz, for each 10 min interval of data. The regular variations of the SRs have been studied using the following parameters: peak amplitudes, peak frequencies, the widths of the resonances, and the PSI for the three first modes. The processed data for the entire measurement period of the station are

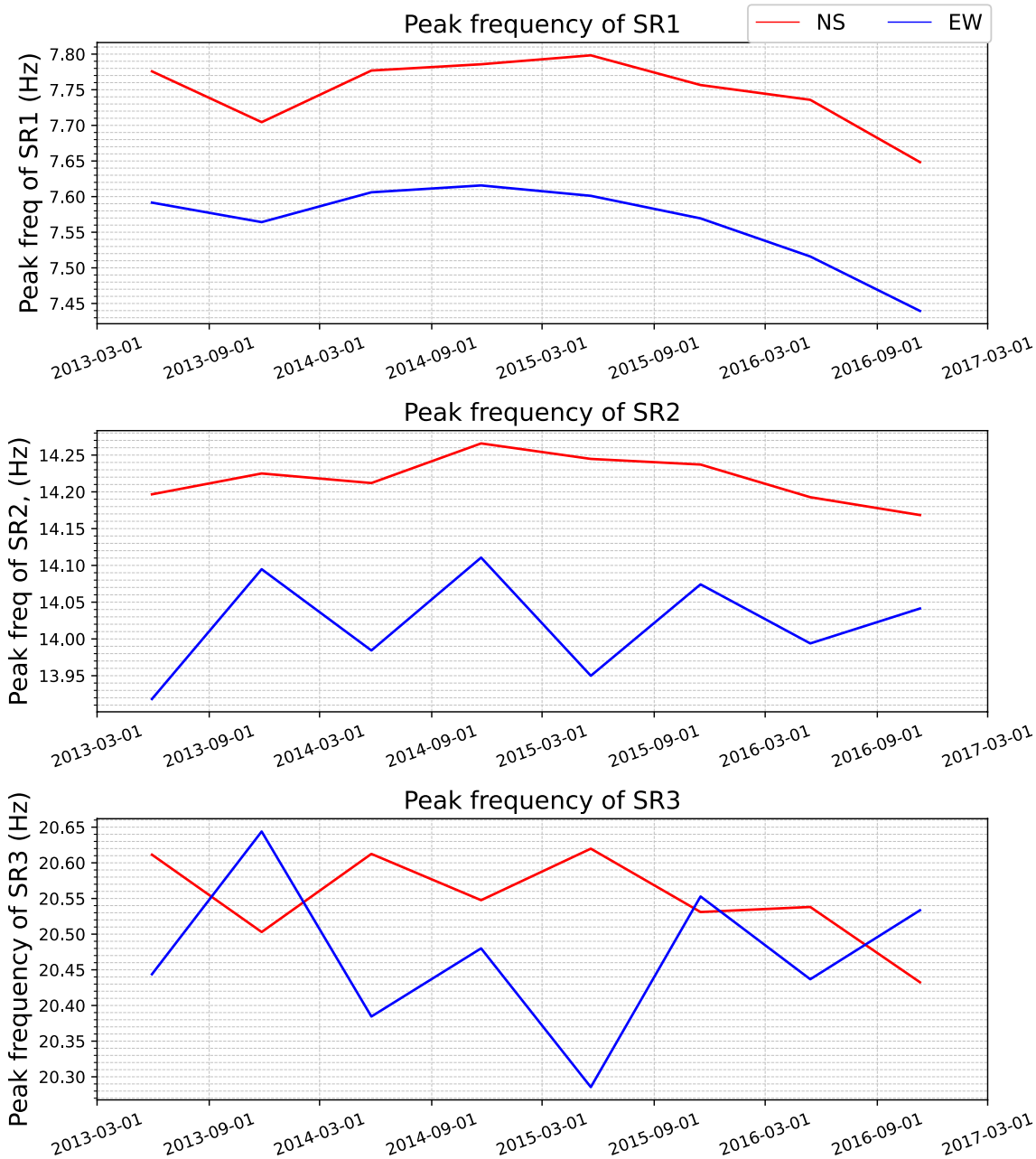


**Figure 11.** Peak frequency daily variations averaged for a 180-day time span for both North-South (red) and East-West (blue) sensors. Each row corresponds to a mode, from the first to the third, respectively.

made public along with this work, and they are presented in a Numpy npz format, which allows easy reading and subsequent processing.

The main findings can be summarized as follows:

1. The general diurnal evolution of the three main storm centers on Earth, Africa, Asia, and America, has been confirmed. There is a predominance of stormy activity in northern hemisphere summer and minimal in winter. The African center exhibits the larger intensity and the Asian center, the longest daily duration.
2. SR2 and SR3 diurnal peak amplitudes of the NS sensor are very sensitive to the African storm center. Diurnal peak amplitudes of SR1-3 in the EW sensor are similar in shape, while for the NS sensor the shape changes for each mode. Regarding the diurnal variation of the frequency, a very different pattern is observed between

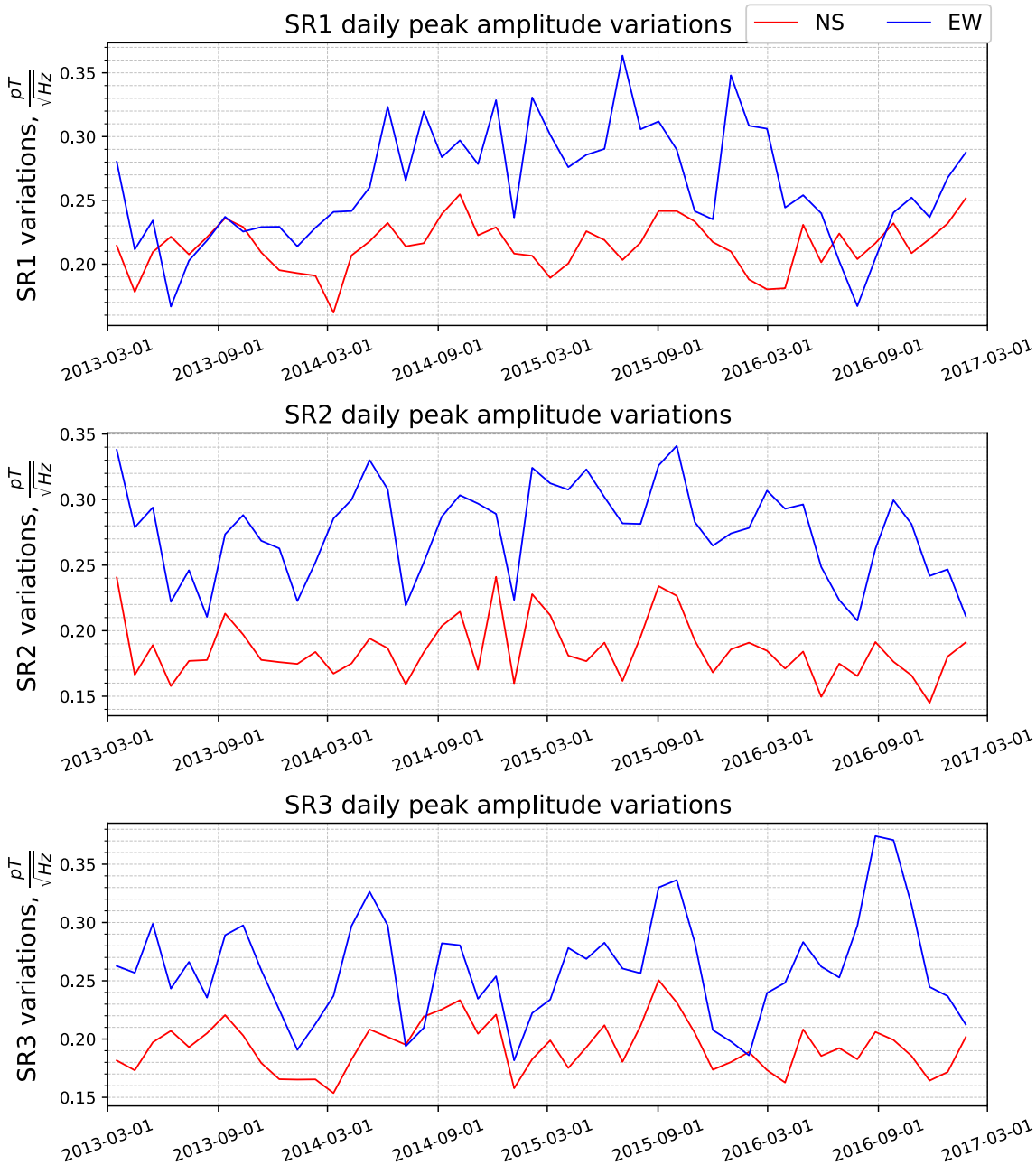


**Figure 12.** Daily variation of the minimum to maximum range of the peak amplitudes, averaged over 30 days, for the three first modes SR1, SR2, and SR3, in the first, the second and the third row, respectively. The North-South sensor is plotted in red, and the East-West sensor is plotted in blue.

the EW and NS sensors, but no strong seasonal variations are observed. Sierra Nevada measurements do not exhibit a transition from winter-type to summer-type variations in the diurnal variations of the peak frequencies. Since that parameter is related to the source-observer distance (e.g., Toledo-Redondo et al., 2016), different stations are expected to exhibit different seasonal patterns. The widths of the resonances are highly fluctuating and it is very difficult to draw conclusions from the measurements. It is observed that the widths are greater for the EW sensor than for the NS one.

3. The peak amplitudes of diurnal averages measured by Sierra Nevada station are roughly half of the peak amplitudes reported by the stations in China. This difference can be attributed to the relative distance of each station to the storm centers. In addition, Sierra Nevada station does not detect a peak in activity

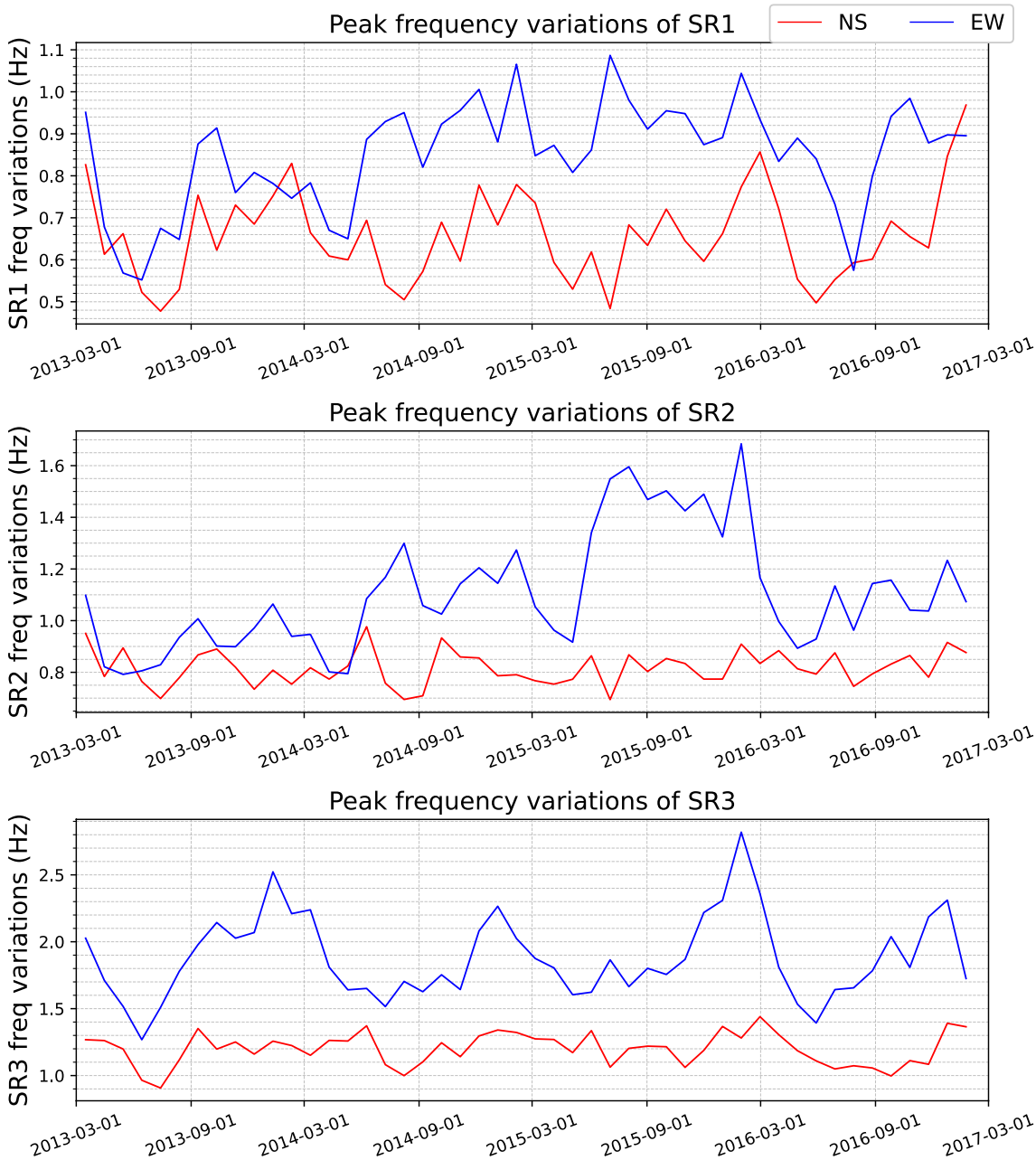


**Figure 13.** Daily variation of the minimum to maximum range of the peak frequencies, averaged over 30 days, for the three first modes SR1, SR2, and SR3, in the first, the second and the third row, respectively. The North-South sensor is plotted in red, and the East-West sensor is plotted in blue.

around 08:00 UT, that activity is shifted to 10:30 UT. This may be explained by the different years considered in our study, but this requires further investigation.

4. The African storm center exhibits maxima of activity during boreal summer, according to our SR records. This is not well supported by global lightning data from satellites (e.g., Blakeslee et al., 2014). A unified database involving several stations around the globe would be desirable to further test these results. The additional activation time, around 0600 UT, only detected by some stations, is observed by the ELF Sierra Nevada station.
5. Diurnal variations of PSI evolve with electromagnetic seasons rather than with astronomical seasons.
6. Predictions by Williams et al. (2021) about the effect of El Niño on SR seem to be detected in the annual diurnal variations of our measurements of the first mode peak amplitude. There are also variations between

EW and NS sensors: the former shows a repeating pattern every month, while the latter has different patterns during summer and winter months.

7. We have obtained results that corroborate some conclusions on an intensification of the SRs during the transition months that precede the super El Niño episode which happened at the end of 2015 and the beginning of 2016, as indicated by Williams et al. (2021). We also find results like those in Koloskov et al. (2020), connected to a tracking of the first mode resonant frequency and the 11-year cycle solar activity, during a period of large solar activity (2011–2017).
8. Daily variations of different parameters are stronger for EW sensor than for NS sensor.

## Data Availability Statement

The data set of this paper will be available from http://hdl.handle.net/10481/71563.

**Acknowledgments**
This work has been supported by the investigation research projects FIS2017-90102-R, of the Ministry of Economy and Competitiveness (MINECO) of Spain, cofinanced by the Fund European Regional Development (FEDER), and PID2020-112805GA-I00, of the Ministry of Science and Innovation of Spain, and the Ministry of Education, Science and Sport of Spain through the FPU grants for PhD studentship (reference: FPU15/04291). Funding for Open Access Charge: Universidad de Granada/CBUA. We are grateful to Parque Nacional Sierra Nevada for providing support to the project.

## References

Aich, V., Holzworth, R., Goodman, S. J., Kuleshov, Y., Price, C., & Williams, E. (2018). Lightning: A new essential climate variable. *Eos*, *99*. https://doi.org/10.1029/2018eo104583

Balser, M., & Wagner, C. A. (1960). Observations of Earth-ionosphere cavity resonances. *Nature*, *188*, 638–641. https://doi.org/10.1038/188638a0

Belyaev, G. G., Schekotov, A. Y., Shvets, A. V., & Nickolaenko, A. P. (1999). Schumann resonances observed using Poynting vector spectra. *Journal of Atmospheric and Solar-Terrestrial Physics*, *61*(10), 751–763. https://doi.org/10.1016/S1364-6826(99)00027-9

Besser, B. P. (2007). Synopsis of the historical development of Schumann resonances. *Radio Science*, *42*(2), RS2S02. https://doi.org/10.1029/2006RS003495

Betz, H. D., Schumann, U., & Laroche, P. (2009). *Lightning: Principles, instruments and applications: Review of modern lightning research*. Springer Netherlands. https://doi.org/10.1007/978-1-4020-9079-0

Blakeslee, R. J., Mach, D. M., Bateman, M. G., & Bailey, J. C. (2014). Seasonal variations in the lightning diurnal cycle and implications for the global electric circuit. *Atmospheric Research*, *135–136*(Supplement C), 228–243. https://doi.org/10.1016/j.atmosres.2012.09.023

Christian, H. J., Blakeslee, R. J., Boccippio, D. J., Boeck, W. L., Buechler, D. E., Driscoll, K. T., et al. (2003). Global frequency and distribution of lightning as observed from space by the Optical Transient Detector. *Journal of Geophysical Research: Atmospheres*, *108*(D1), ACL 4-1-ACL 4-15. https://doi.org/10.1029/2002jd002347

Fornieles-Callejón, J., Salinas, A., Toledo-Redondo, S., Portí, J., Méndez, A., Navarro, E. A., et al. (2015). Extremely low frequency band station for natural electromagnetic noise measurement. *Radio Science*, *50*, 191–201. https://doi.org/10.1002/2014RS005567

Füllekrug, M., & Fraser-Smith, A. C. (1997). Global lightning and climate variability inferred from ELF magnetic field variations. *Geophysical Research Letters*, *24*(19), 2411–2414. https://doi.org/10.1029/97GL02358

Koloskov, A. V., Nickolaenko, A. P., Yampolsky, Y. M., Hall, C., & Budanov, O. V. (2020). Variations of global thunderstorm activity derived from the long-term Schumann resonance monitoring in the Antarctic and in the Arctic. *Journal of Atmospheric and Solar-Terrestrial Physics*, *201*, 105231. https://doi.org/10.1016/j.jastp.2020.105231

Kulak, A., Kubisz, J., Michalec, A., Zięba, S., & Nieckarz, Z. (2003). Solar variations in extremely low frequency propagation parameters: 2. Observations of Schumann resonances and computation of the ELF attenuation parameter. *Journal of Geophysical Research*, *108*(A7). https://doi.org/10.1029/2002JA009305

Melnikov, A., Price, C., Sátori, G., & Füllekrug, M. (2004). Influence of solar terminator passages on Schumann resonance parameters. *Journal of Atmospheric and Solar-Terrestrial Physics*, *66*(13), 1187–1194. https://doi.org/10.1016/j.jastp.2004.05.014

Nickolaenko, A. P., & Hayakawa, M. (2002). *Resonances in the Earth-ionosphere cavity*. Kluwer Academic.

Nickolaenko, A. P., & Hayakawa, M. (2014). *Schumann resonance for Tyros*. Springer.

Nickolaenko, A. P., Hayakawa, M., & Hobara, Y. (1999). Long-term periodical variations in global lightning activity deduced from the Schumann resonance monitoring. *Journal of Geophysical Research*, *104*(D22), 27585–27591. https://doi.org/10.1029/1999jd900791

Nickolaenko, A. P., Koloskov, A. V., Hayakawa, M., Yampolski, Y. M., Budanov, O. V., & Korepanov, V. E. (2015). 11-year solar cycle in Schumann resonance data as observed in Antarctica. *Sun and Geosphere*, *10*(1), 39–49.

Nickolaenko, A. P., & Rabinowicz, L. M. (1995). Study of the annual changes of global lightning distribution and frequency variations of the first Schumann resonance mode. *Journal of Atmospheric and Terrestrial Physics*, *57*(11), 1345–1348. https://doi.org/10.1016/0021-9169(94)00114-4

Nickolaenko, A. P., Sátori, G., Zieger, B., Rabinowicz, L. M., & Kudintseva, I. G. (1998). Parameters of global thunderstorm activity deduced from the long-term Schumann resonance records. *Journal of Atmospheric and Solar-Terrestrial Physics*, *60*(3), 387–399. https://doi.org/10.1016/S1364-6826(97)00121-1

Nickolayenko, A. P., Shvets, A. V., & Hayakawa, M. (2016). Extremely low frequency (ELF) radio wave propagation: A review. *International Journal of Electronics and Applied Research (IJEAR)*, *3*(2), 91.

Ondrášková, A., Kostecký, P., Ševčík, S., & Rosenberg, L. (2007). Long-term observations of Schumann resonances at Modra observatory. *Radio Science*, *42*(2), RS2S09. https://doi.org/10.1029/2006RS003478

Ondrášková, A., Ševčík, S., & Kostecký, P. (2011). Decrease of Schumann resonance frequencies and changes in the effective lightning areas toward the solar cycle minimum of 2008–2009. *Journal of Atmospheric and Solar-Terrestrial Physics*, *73*(4), 534–543. https://doi.org/10.1016/j.jastp.2010.11.013

Ouyang, X. Y., Xiao, Z., Hao, Y. Q., & Zhang, D. H. (2015). Variability of Schumann resonance parameters observed at low latitude stations in China. *Advances in Space Research*, *56*(7), 1389–1399. https://doi.org/10.1016/j.asr.2015.07.006

Price, C. (2000). Evidence for a link between global lightning activity and upper tropospheric water vapour. *Nature*, *406*(6793), 290–293. https://doi.org/10.1038/35018543

Price, C. (2016). ELF electromagnetic waves from lightning: The Schumann resonances. *Atmosphere*, *7*(9), 116. https://doi.org/10.3390/atmos7090116

Price, C., & Melnikov, A. (2004). Diurnal, seasonal and inter-annual variations in the Schumann resonance parameters. *Journal of Atmospheric and Solar-Terrestrial Physics*, *66*(13–14), 1179–1185. https://doi.org/10.1016/j.jastp.2004.05.004

Rodríguez-Camacho, J., Fornieles, J., Carrión, M. C., Portí, J., Toledo-Redondo, S., & Salinas, A. (2018). On the need of a unified methodology for processing Schumann resonance measurements. *Journal of Geophysical Research: Atmospheres*, *123*(23), 13277–13290. https://doi.org/10.1029/2018JD029462

Sátori, G. (1996). Monitoring Schumann resonances-II. Daily and seasonal frequency variations. *Journal of Atmospheric and Terrestrial Physics*, *58*(13), 1483–1488. https://doi.org/10.1016/0021-9169(95)00146-8

Sátori, G. (2003). *On the dynamics of the North–South seasonal migration of global lightning*. *Paper presented at 12th international conference on atmospheric electricity, Versailles, France*. Global Lightning and Climate.

Sátori, G., Williams, E., & Lemperger, I. (2009). Variability of global lightning activity on the ENSO time scale. *13th International Conference on Atmospheric Electricity ICAE 2007*, *91*(2–4), 500–507. https://doi.org/10.1016/j.atmosres.2008.06.014

Sátori, G., Williams, E., & Mushtak, V. (2005). Response of the Earth–ionosphere cavity resonator to the 11-year solar cycle in X-radiation. *Journal of Atmospheric and Solar-Terrestrial Physics*, *67*(6), 553–562. https://doi.org/10.1016/j.jastp.2004.12.006

Sátori, G., Williams, E. R., & Boccippio, D. J. (2003). *On the dynamics of the North – South seasonal migration of global lightning*. *Paper presented at AGU Fall Meeting, San Francisco, December 8–12*. Abstract no.: AE32A-0167.

Sátori, G., & Zieger, B. (1996). Spectral characteristics of Schumann resonances observed in central Europe. *Journal of Geophysical Research: Atmospheres*, *101*(D23), 29663–29669. https://doi.org/10.1029/96JD00549

Sátori, G., & Zieger, B. (1999). El Niño related meridional oscillation of global lightning activity. *Geophysical Research Letters*, *26*(10), 1365–1368. https://doi.org/10.1029/1999gl900264

Schumann, W. O. (1952). Über die stralungslosen Eigenschwingungen einer leitenden Kugel die von einer Luftschicht und einer Ionospärenhle umgeben ist. *Zeitschrift für Naturforschung*, *7a*, 149–154. https://doi.org/10.1515/zna-1952-0202

Sekiguchi, M., Hayakawa, M., Nickolaenko, A. P., & Hobara, Y. (2006). Evidence on a link between the intensity of Schumann resonance and global surface temperature. *Annales Geophysicae*, *24*(7), 1809–1817. https://doi.org/10.5194/angeo-24-1809-2006

Simões, F., Pfaff, R., Berthelier, J.-J., & Klenzing, J. (2012). A review of low frequency electromagnetic wave phenomena related to tropospheric-ionospheric coupling mechanisms. *Space Science Reviews*, *168*(1–4), 551–593. https://doi.org/10.1007/s11214-011-9854-0

Surkov, V., & Hayakawa, M. (2014). *Ultra and extremely low frequency electromagnetic fields*. Springer.

Toledo-Redondo, S., Parrot, M., & Salinas, A. (2012). Variation of the first cut-off frequency of the Earth-ionosphere waveguide observed by DEMETER. *Journal of Geophysical Research*, *117*, A04321. https://doi.org/10.1029/2011JA017400

Toledo-Redondo, S., Salinas, A., Fornieles, J., Portí, J., & Lichtenegger, H. I. M. (2016). Full 3-D TLM simulations of the Earth-ionosphere cavity: Effect of conductivity on the Schumann resonances. *Journal of Geophysical Research: Space Physics*, *121*, 5579–5593. https://doi.org/10.1002/2015JA022083

Toledo-Redondo, S., Salinas, A., Portí, J., Morente, J. A., Fornieles, J., Méndez, A., et al. (2010). Study of Schumann resonances based on magnetotelluric records from the Western Mediterranean and Antarctica. *Journal of Geophysical Research*, *115*, D22114. https://doi.org/10.1029/2010JD014316

Williams, E., Bozóki, T., Sátori, G., Price, C., Steinbach, P., Guha, A., et al. (2021). Evolution of global lightning in the transition from cold to warm phase preceding two super El Niño events. *Journal of Geophysical Research: Atmospheres*, *126*(3), e2020JD033526. https://doi.org/10.1029/2020jd033526

Williams, E., Guha, A., Boldi, R., Christian, H., & Buechler, D. (2019). Global lightning activity and the hiatus in global warming. *Journal of Atmospheric and Solar-Terrestrial Physics*, *189*, 27–34. https://doi.org/10.1016/j.jastp.2019.03.011

Williams, E. R. (1992). The Schumann resonance: A global tropical thermometer. *Science*, *256*(5060), 1184–1187. https://doi.org/10.1126/science.256.5060.1184

Williams, E. R. (2005). Lightning and climate: A review. *Atmospheric Research*, *76*(1–4), 272–287. https://doi.org/10.1016/j.atmosres.2004.11.014

Yatsevich, E. I., Nickolaenko, A. P., & Pechonaya, O. B. (2008). Diurnal and seasonal variations in the intensities and peak frequencies of the first three Schumann-resonance modes. *Radiophysics and Quantum Electronics*, *51*(7), 528–538. https://doi.org/10.1007/s11141-008-9056-0

Yatsevich, E. I., Nickolaenko, A. P., Shvets, A. V., & Rabinowicz, L. M. (2005). Two component model of the Schumann resonance signal. *Telecommunications and Radio Engineering*, *64*(7–12). https://doi.org/10.1615/telecomradeng.v64.i10.100

Zhou, H., Yu, H., Cao, B., & Qiao, X. (2013). Diurnal and seasonal variations in the Schumann resonance parameters observed at Chinese observatories. *Journal of Atmospheric and Solar-Terrestrial Physics*, *98*, 86–96. https://doi.org/10.1016/j.jastp.2013.03.021